PLANA3R: Zero-shot Metric Planar 3D Reconstruction via Feed-Forward Planar Splatting

Changkun Liu[1,2*] **Bin Tan**[2*] **Zeran Ke**[2,3] **Shangzhan Zhang**[2,4] **Jiachen Liu**[5] **Ming Qian**[2,3]

Nan Xue[2†] **Yujun Shen**[2] **Tristan Braud**[1]

[1]The Hong Kong University of Science and Technology [2]Ant Group

[3]Wuhan University [4]Zhejiang University [5]The Pennsylvania State University
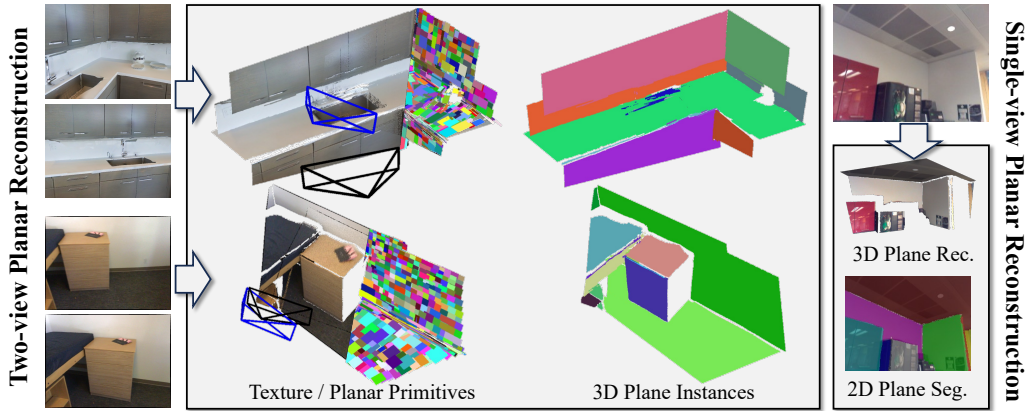
Figure 1: Our proposed PLANA3R learns to predict planar 3D primitives and metric-scale relative poses, providing a compact 3D representation of two-view input images with accurate pose estimation, surface geometry, and semantically meaningful 2D & 3D planar segmentation—all in one pass. As a side output, our model also performs well on single-view planar 3D reconstruction.

Abstract

This paper addresses metric 3D reconstruction of indoor scenes by exploiting their inherent geometric regularities with compact representations. Using planar 3D primitives – a well-suited representation for man-made environments – we introduce PLANA3R, a pose-free framework for metric Planar 3D Reconstruction from unposed two-view images. Our approach employs Vision Transformers to extract a set of sparse planar primitives, estimate relative camera poses, and supervise geometry learning via planar splatting, where gradients are propagated through high-resolution rendered depth and normal maps of primitives. Unlike prior feedforward methods that require 3D plane annotations during training, PLANA3R learns planar 3D structures without explicit plane supervision, enabling scalable training on large-scale stereo datasets using only depth and normal annotations. We validate PLANA3R on multiple indoor-scene datasets with metric supervision and demonstrate strong generalization to out-of-domain indoor environments across diverse tasks under metric evaluation protocols, including 3D surface reconstruction, depth estimation, and relative pose estimation. Furthermore, by formulating with planar 3D representation, our method emerges with the ability for accurate plane segmentation. The project page is available at: `https://lck666666.github.io/plana3r/`.

---

*Equal Contribution.

†Corresponding author.

1   Introduction

Indoor environments are the primary setting where humans spend most of their daily lives. Yet, computationally creating digital twins of these 3D spaces from captured images remains challenging. Factors such as the difficulty of accurate camera pose estimation from indoor images [28, 11, 1] and structural distortions in the resulting 3D reconstructions [22, 12, 21] hinder the development of robust, accurate, and user-friendly solutions for replicating indoor scenes in the digital world.

As indoor scenes are typically rich in planar structures such as floors, ceilings, and walls, as well as planar furniture like tables and cabinets, planar primitives are well-suited representations for the accurate 3D reconstruction of indoor scenes. As a result, there has been significant interest among the research community in planar 3D reconstruction in recent years. Planar reconstruction approaches include feedforward solutions in monocular [40, 16, 27, 24, 18, 42] and two-view [11, 1, 28] settings, and per-scene optimization approaches [29, 38, 3, 9] that leverage posed multi-view inputs with the assistance of the feedforward models were studied. However, these approaches face two key limitations:

- **Annotation dependence for feedforward methods**: Learning feedforward models [36, 24, 28] typically requires accurate plane masks and 3D plane annotations from monocular or binocular inputs. This reliance on dense annotations limits generalizability and thus impairs zero-shot performance on out-of-distribution data.

- **Pose dependence for optimization-based methods**: Per-scene optimization techniques [29, 9, 38, 3] depend on accurately posed multi-view, densely-captured images, which are not always available and would lead to either undermining reconstruction quality or limited usage scenarios. Furthermore, these methods cannot handle several sparse pose-free views or just a pair of pose-free views.

This paper focuses on two-view planar 3D reconstruction, one of the most fundamental tasks in structured indoor scene modeling. We aim to eliminate the reliance on dense plane-level annotations and accurate multi-view camera poses, addressing the limitations discussed above. Inspired by recent advancements in 3D foundation models [33, 14, 31, 32, 30, 37, 41], we show that feedforward, pose-free, and zero-shot generalizable planar 3D reconstruction from unposed stereo pairs is both feasible and effective through our proposed method, PLANA3R.

PLANA3R is built upon Vision Transformers [7], which process stereo image pairs to jointly learn 3D planar primitives and relative camera poses at scale. Rather than relying on explicit planar 3D annotations, we leverage depth and normal maps[3], which are more readily available in existing two-view datasets at scale, as supervision signals to train the Transformer-based model. To this end, we adopt the differentiable planar rendering technique from PlanarSplatting [29] to generate high-resolution rendered depth and normal maps, and then compare them with the corresponding ground truth to guide learning through gradient-based optimization. Once the model is trained, our method generates a set of 3D planar primitives that approximate indoor scenes far more efficiently than per-scene optimization methods [29, 9, 38, 3]. As shown in Fig. 1, our trained PLANA3R computes metric pose and planar primitives in a single feed-forward inference, resulting in a compact representation of indoor scenes with accurate geometry and meaningful semantics.

Given that indoor environments are constructed by humans, and the dimensions of human-scale objects tend to follow similar distributions across different scenes, we consider that planar 3D representation inherently possesses the potential to predict metric 3D geometry directly. Therefore, during training data preparation, we pay particular attention to preserving the metric scale of both depth maps and relative camera poses. In total, four million training data from ScanNetV2 [4], ScanNet++ [39], ARKitScenes [5], and Habitat [23] have been prepared to train our PLANA3R model with metric scales.

PLANA3R exhibits a strong generalization ability to out-of-domain indoor environments in terms of depth estimation, 3D surface reconstruction, and relative pose estimation. Benefiting from the planar-based representation we used, our model also empowers the capacity to provide promising instance-wise planar segmentation, enriching the semantics of 3D reconstruction without the need for

---

[3]For the dataset that only contains depth maps, the Metric3Dv2 [10] is applied to generate pseudo labels as the normal maps. Please refer to Sec. 4.2 for details.

plane masks. Furthermore, we argue that indoor scenes are particularly well-suited for training metric 3D vision foundation models. The regular geometry and semantic consistency of indoor environments provide an ideal context for developing models that generalize across scenes and accurately estimate metric information.

2 Related Work

In this section, we briefly summarize the recent developments on the 3D reconstruction of indoor scenes in two aspects of planar representation and feedforward modeling.

2.1 Indoor Planar 3D Reconstruction

Given the strong planarity of indoor scenes, planar surface reconstruction has been extensively studied in the literature [17, 27, 16, 24, 1, 40, 11, 28, 34, 36, 29, 9, 38]. Among existing methods, feedforward approaches [24, 27, 36, 28, 11] are particularly appealing due to their simplified computation pipelines powered by neural networks. However, most of these methods focus on in-domain testing using small or moderate-scale datasets. A major limitation is the scarcity of large-scale, high-quality 3D planar annotations, which constrains supervision and limits the generalization ability of models trained on such data.

For instance, methods like SparsePlanes [11], PlaneFormers [1], and NOPE-SAC [28] rely on single-view 3D plane annotations and two-view 3D plane correspondences as supervision, restricting usable data sources to ScanNetV2 [4] and Matterport3D [2] datasets and requiring complex data preprocessing pipelines. To address this, our work improves data accessibility by leveraging PlanarSplatting [29] as an alternative to the manually-annotated planar supervisions. This makes it possible to train models on large-scale 3D datasets by learning sparse planar primitives without requiring explicit plane-level annotations.

2.2 Feed-forward Stereo Foundation Models for 3D Reconstruction

The rise of large-scale training has significantly transformed the landscape of 3D reconstruction [33, 14, 32, 41, 31, 30, 37]. Recently, DUSt3R [33] introduced a feedforward framework that predicts dense point clouds from stereo image pairs without requiring known camera poses. Building on this, MASt3R [14] further enhances performance by generating point clouds in metric space. Several follow-up works have since explored ways to improve both scene geometry estimation [32, 30] and camera pose prediction [6, 41]. However, these methods typically assume that scene geometry can be effectively represented by densely sampled 3D points, which introduces redundancy when modeling structured environments. In contrast, we adopt more abstract planar primitives to express structured scenes with the best pursuit of compactness and efficiency in representation.

While our method shares architectural similarities with DUSt3R [33] and MASt3R [14], notably the use of Vision Transformers [7], we depart from their dense point-based representations. Instead, we focus on exploiting the strong planar regularities characteristic of indoor scenes by adopting a structured planar representation. We demonstrate that this formulation, based on the use of sparse planar primitives, can represent structured scenes more compactly and efficiently while also enabling the extraction of instance-level planar semantics.

3 Method

PLANA3R is a transformer-based model for two-view metric 3D reconstruction, using sparse 3D planar primitives as a scene representation. Given two pose-free images from the same scene, along with known intrinsics, PLANA3R predicts their relative camera pose and infers a set of 3D planar primitives in a single feed-forward pass. We build upon planar primitives introduced in PlanarSplatting [29], and leverage its CUDA-based differentiable renderer for supervision. PlanarSplatting is a core component of PLANA3R, providing ultra-fast and accurate reconstruction of planar surfaces in indoor scenes from multi-view images. Instead of detecting or matching planes in 2D or 3D, it directly splats 3D planar primitives into dense depth and normal maps via differentiable, CUDA-accelerated rasterization.

This allows PLANA3R to be trained directly from monocular depth and normal labels, without requiring explicit plane annotations. Sparse planar primitives offer a more compact and semantically meaningful alternative to dense point clouds or 3D Gaussian Splatting (3DGS) [13], particularly in structured indoor environments. They approximate scene geometry with high fidelity and support the rendering of dense, consistent depth and normal maps. Moreover, the explicit structure of primitives facilitates downstream tasks such as plane extraction and segmentation.

The predicted primitives can be further merged into coherent planar surfaces to support both 3D reconstruction and segmentation. We detail the task setup and notation in Sec. 3.1, describe our architecture in Sec. 3.2, outline training objectives in Sec. 3.3, and explain the primitive merging process in Sec. 3.4.

3.1 Task Setting and Notation

An overview of PLANA3R is shown in Fig. 2. The input consists of two images $I^1, I^2 \in \mathbb{R}^{3 \times H \times W}$ with camera intrinsics $\mathbf{K}^1$ and $\mathbf{K}^2$. Our goal is to train a network $\mathcal{F}$ outputs a set of sparse 3D planar primitives and the 6-DoF relative camera pose P_{rel}. P_{rel} is represented by the quaternion $\mathbf{q} \in \mathbb{R}^4$ and translation $\mathbf{t} \in \mathbb{R}^3$:
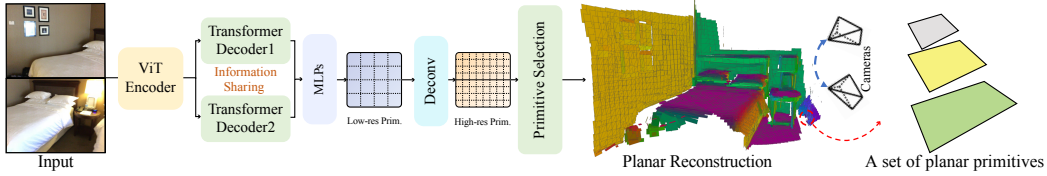

Figure 2: Overview of our PLANA3R. Given two images captured from the same scene, PLANA3R outputs a set of 3D planar primitives and 6-DoF relative camera pose P_{rel} in metric scale. PLANA3R does not perform per-pixel primitive prediction. Instead, it employs a deconvolution network to predict primitives at two distinct resolutions, based on the patch divisions from the ViT encoder. During both training and inference phases, we selectively integrate low-resolution and high-resolution primitives, resulting in a highly compact and expressive representation. Note that even for high-resolution primitives, their total number is only $\frac{H}{8} \times \frac{W}{8}$, which remains highly sparse.

$$\mathcal{F} : \left\{ (I^i, \mathbf{K}^i) \right\}_{i=1,2} \Rightarrow \left\{ (d_\pi^i, \ \mathbf{r}_\pi^i, \ \mathbf{q}_\pi^{i,j}) \right\}_{i=1,2; \ j=1}^{N_i}, \ P_{\text{rel}}, \tag{1}$$

where $\mathbf{q}_\pi^{i,j}$ denotes the quaternion of a planar primitive generated from image I^i, represented in the coordinate frame of the camera j. $d_\pi^i \in \mathbb{R}_+^1$ denotes the depth of a planar primitive center associated with image I^i. N_i denotes the number of planar primitives associated with image I^i. $\mathbf{r}_\pi = (\mathbf{r}_\pi^x, \mathbf{r}_\pi^y), \mathbf{r}_\pi \in \mathbb{R}_+^2$ denotes the plane radii. $\mathbf{r}_\pi^i$ refers to the radii array of a planar primitive associated with image I^i. In our training setup, we fix $j = 1$, treating I^1 as the reference frame. Accordingly, the ground-truth camera pose of I^1 is set to the 4×4 identity matrix. Then, the primitive centers $\mathbf{c}_\pi^i \in \mathbb{R}^3$ from both I^1 and I^2 are transformed into the coordinate frame of the camera $j = 1$ using the corresponding intrinsics $\mathbf{K}^i$, depth d_π^i, and camera poses. Following PlanarSplatting [29], we define the same positive direction of the X-axis/Y-axis of the 3D planar primitive and calculate the normal of the planar primitive $\mathbf{n}_\pi \in \mathbb{R}^3$ as:

$$\mathbf{n}_\pi = \mathbf{R}(\mathbf{q}_\pi)[0, 0, 1]^T, \tag{2}$$

where $\mathbf{R}(\mathbf{q}_\pi)$ converts $\mathbf{q}_\pi$ to the rotation matrix.

Input images $\{I^i\}_{i=1,2}$ are first encoded in a Siamese fashion using a ViT encoder [7], producing feature maps $\{F^i\}_{i=1,2} \in \mathbb{R}^{\frac{H}{16} \times \frac{W}{16} \times D_{\text{enc}}}$. These features are then processed by two transformer decoders with cross-attention to produce low-resolution decoder embeddings $\{G_{\text{low}}^i\}_{i=1,2} \in \mathbb{R}^{\frac{H}{16} \times \frac{W}{16} \times D_{\text{dec}}}$. A separate head regresses the relative camera pose P_{rel} from the concatenated low-resolution features $\{G_{\text{low}}^i\}_{i=1,2}$. This partial architecture of our network $\mathcal{F}$ is inspired by some stereo 3D vision models [33, 14, 6, 35]. The core innovation of our method lies in the sparse primitive prediction architecture outlined in Sec. 3.2 and Sec. 3.3.

4

Compared to per-pixel 3D Gaussian Splatting and dense 3D point regression methods, our approach leverages the inherent compactness of planar primitives. Many pixels naturally form coherent planar regions in structured indoor environments, making per-pixel representations unnecessarily redundant. Although non-planar or texture-rich areas may require finer approximations with smaller primitives, such cases are relatively rare. To achieve a more compact and efficient geometric representation using fewer primitives, we propose a *hierarchical primitive prediction architecture* (HPPA) to fit the scene using planar primitives, enabling compact modeling of scene geometry with sparse primitives.

3.2 Hierarchical Primitive Prediction Architecture

From $\{G_{\text{low}}^i\}_{i=1,2}$, three regression heads first predict low-resolution patched planar primitives $\left\{(d_\pi^i,\ \mathbf{r}_\pi^i,\ \mathbf{q}_\pi^{i,j})\right\}_{i=1,2;\ j=1}^{\frac{H}{16}\times\frac{W}{16}}$. To obtain higher-resolution features, we apply a deconvolution network to upsample $\{G_{\text{low}}^i\}_{i=1,2}$, generating $\{G_{\text{high}}^i\}_{i=1,2}\ \in\ \mathbb{R}^{\frac{H}{8}\times\frac{W}{8}\times D_{\text{dec}}}$. The same three heads then regress high-resolution patched planar primitives $\left\{(d_\pi^i,\ \mathbf{r}_\pi^i,\ \mathbf{q}_\pi^{i,j})\right\}_{i=1,2;\ j=1}^{\frac{H}{8}\times\frac{W}{8}}$. The primary challenge then becomes determining which image regions require low-resolution planar primitives and which benefit from higher-resolution primitives. To address this, we propose a simple yet effective heuristic that avoids the need for additional learning.

Our approach is based on the observation that regions exhibiting significant variations in normals require a greater number of smaller planar primitives for accurate fitting, whereas areas with minimal changes in normals can be effectively represented by fewer planar primitives with larger radii. For each input image, using d_π in predicted primitives, we derive the patched depth maps: $\mathbf{D}_{\text{low}}^{\text{patch}} \in \mathbb{R}^{1\times\frac{H}{16}\times\frac{W}{16}}$ and $\mathbf{D}_{\text{high}}^{\text{patch}} \in \mathbb{R}^{1\times\frac{H}{8}\times\frac{W}{8}}$. Similarly, using q_π in predicted primitives and Eq. (2), two different patched normal maps are obtained: $\mathbf{N}_{\text{low}}^{\text{patch}} \in \mathbb{R}^{3\times\frac{H}{16}\times\frac{W}{16}}$ and $\mathbf{N}_{\text{high}}^{\text{patch}} \in \mathbb{R}^{3\times\frac{H}{8}\times\frac{W}{8}}$. We compute the gradient magnitude for each pixel in the low-resolution predicted normal patches $\mathbf{N}_{\text{low}}^{\text{patch}}$ of size $\frac{H}{16}\times\frac{W}{16}$, and selectively use the high-resolution planar primitives of size $\frac{H}{8}\times\frac{W}{8}$ only for those pixels whose gradients exceed a predefined threshold g_{th} during rendering. To combine the low- and high-resolution primitives, we use binary masks to merge only the valid patches from both resolutions, rather than directly using all predicted primitives. We provide more details in Fig. 12 (b).

3.3 Training Losses and Training Strategies

For input images $\{I^i\}_{i=1,2}$, PLANA3R generates planar primitives at both low and high resolutions. Specifically, the low-resolution primitives are represented as $\left\{(d_\pi^i,\mathbf{r}_\pi^i,\mathbf{q}_\pi^{i,j})\right\}_{i=1,2;\ j=1}^{\frac{H}{16}\times\frac{W}{16}}$, while the high-resolution primitives are given by $\left\{(d_\pi^i,\mathbf{r}_\pi^i,\mathbf{q}_\pi^{i,j})\right\}_{i=1,2;\ j=1}^{\frac{H}{8}\times\frac{W}{8}}$. Due to the randomness of initialization at the beginning of training, the initial planar primitives often lie outside the viewable range defined by the ground-truth (GT) camera poses. As a result, directly applying the differentiable planar primitive rendering from PlanarSplatting [29] becomes ineffective for optimizing these learnable primitives. To address these challenges and facilitate training, we introduce a patch loss designed to stabilize primitive positioning and orientation:

$$\mathcal{L}_*^{\text{patch}} = \alpha_1 \left\| 1 - \left(\mathbf{N}_*^{\text{patch}}\right)^\top \mathbf{N}_*^{\text{r. gt}}\right\|_1 + \alpha_1 \left\|\mathbf{N}_*^{\text{patch}} - \mathbf{N}_*^{\text{r. gt}}\right\|_1 + \alpha_2 \left\|\mathbf{D}_*^{\text{patch}} - \mathbf{D}_*^{\text{r. gt}}\right\|_1, \quad (3)$$

where $* \in \{\text{low}, \text{high}\}$, α_1 and α_2 are loss weights. Here, $\mathbf{D}_*^{\text{r. gt}}$ and $\mathbf{N}_*^{\text{r. gt}}$ are derived by resizing the ground-truth depth maps $\mathbf{D}^{\text{gt}} \in \mathbb{R}^{1\times H\times W}$ and normal maps $\mathbf{N}^{\text{gt}} \in \mathbb{R}^{3\times H\times W}$ to dimensions $\frac{H}{16}\times\frac{W}{16}$ and $\frac{H}{8}\times\frac{W}{8}$, respectively. The patch loss in the initial warm-up training stage aids in stabilizing the spatial positioning and orientation of the primitives.

After the warm-up phase, we introduce a rendering loss. We render depth and normal maps from both primitive sets. Unlike the patch loss in Eq. (3), which supervises only depth and orientation, the rendering loss in Eq. (4) compares rendered and ground-truth maps using PlanarSplatting's rasterization at full resolution ($H \times W$). This enables gradient flow to refine primitive radii and improves geometric fidelity. Specifically, $\mathbf{N}_{\text{low}}^{\text{render}} \in \mathbb{R}^{3\times H\times W}$ and $\mathbf{D}_{\text{low}}^{\text{render}} \in \mathbb{R}^{1\times H\times W}$ are rendered from $\frac{H}{16}\times\frac{W}{16}$ low-resolution primitives, while $\mathbf{N}_{\text{high}}^{\text{render}} \in \mathbb{R}^{3\times H\times W}$ and $\mathbf{D}_{\text{high}}^{\text{render}} \in \mathbb{R}^{1\times H\times W}$ originate from $\frac{H}{8}\times\frac{W}{8}$ high-resolution primitives. As discussed in Sec. 3.2, during the inference stage,

rendering all regions of the image using all high-resolution primitives is redundant. Therefore, during training, we select some low-resolution primitives and some high-resolution primitives for rendering. We compute the gradient magnitude for each pixel in low-resolution $\mathbf{N}_{\text{low}}^{\text{patch}}$ and use high-resolution planar primitives only for those pixels whose gradients exceed a predefined threshold g_{th} during rendering. $\mathbf{N}_{\text{selected}}^{\text{render}} \in \mathbb{R}^{3 \times H \times W}$ and $\mathbf{D}_{\text{selected}}^{\text{render}} \in \mathbb{R}^{1 \times H \times W}$ are rendered from N selected primitives, $\frac{H}{16} \times \frac{W}{16} \leq N \leq \frac{H}{8} \times \frac{W}{8}$.

To optimize these learnable planar primitives, our PLANA3R is trained in a supervised manner based on the differentiable planar primitive rendering in PlanarSplatting:

$$\mathcal{L}_*^{\text{render}} = \beta_1 \left\| 1 - \left(\mathbf{N}_*^{\text{render}} \right)^\top \mathbf{N}^{\text{gt}} \right\|_1 + \beta_1 \left\| \mathbf{N}_*^{\text{render}} - \mathbf{N}^{\text{gt}} \right\|_1 + \beta_2 \left\| \mathbf{D}_*^{\text{render}} - \mathbf{D}^{\text{gt}} \right\|_1, \qquad (4)$$

where $* \in \{\text{low}, \text{high}, \text{selected}, \}$ and β_1, β_2 balance the loss magnitudes for stable training.

For the predicted relative pose $P_{\text{rel}} = [\mathbf{t}, \mathbf{q}]$, we use MSE loss and relative angle loss to provide supervision:

$$\mathcal{L}^{\text{pose}} = \gamma_1 \left\| \mathbf{t}^{\text{gt}} - \mathbf{t} \right\|_1 + \gamma_2 \left\| \mathbf{q}^{\text{gt}} - \frac{\mathbf{q}}{\|\mathbf{q}\|} \right\|_1 + \gamma_3 (1 - \frac{\mathbf{t} \cdot \mathbf{t}^{\text{gt}}}{\|\mathbf{t}\| \|\mathbf{t}^{\text{gt}}\|}), \qquad (5)$$

where $\gamma_1, \gamma_2, \gamma_3$ are loss weights for different items.

Note that our model focuses on metric reconstruction. Therefore, we do not apply normalization to the training labels. Instead, we use metric depth maps and metric poses for supervision in Eq. (3), Eq. (4), and Eq. (5).

3.4 3D Plane Merge

Given a pair of input images, once the collection of 3D planar primitives is predicted, we perform a similar merging in PlanarSplatting by setting thresholds for the normal and distance errors between each pair of primitives. This process enables the extraction of semantic information for each plane and yields the final planar surface reconstruction. We provide more details in Appendix A.2.

4 Experiment

4.1 Implementation Details

We initialize the ViT encoder and the transformer decoder's part of PLANA3R model with DUSt3R's pre-trained 512-DPT weights. Training is performed using the AdamW optimizer [19] with a learning rate starting at 1×10^{-4} and decaying to 1×10^{-6}. The model is trained for a total of 256 GPU-days on NVIDIA H20 GPUs, with a per-GPU batch size of 6. Training starts with a one-epoch warm-up phase that optimizes only the losses in Eq. (3) and Eq. (5), followed by 10 epochs incorporating all three losses at an input resolution of 512×384. During both training and testing, we set the gradient threshold g_{th} for merging high- and low-resolution primitives to 0.5. Additional details are provided in the *supplementary materials*.

4.2 Datasets

Since PLANA3R targets structured indoor scenes, we train it on a combination of four public indoor-scene datasets: ScanNetV2 [4], ScanNet++ [39], ARKitScenes [5], and Habitat [23]. From these datasets, we construct approximately four million image pairs. Pseudo GT normal maps are generated using Metric3Dv2 [10], while GT depth maps are directly taken from the datasets. For evaluation, we use ScanNetV2, Matterport3D [2], NYUv2-Plane [20, 15], and Replica [26] as test sets. Among these test sets, except for ScanNetV2, the remaining three datasets demonstrate the generalization capability of our model across different datasets. We also evaluate on 7Scenes [25] in Appendix A.1.

4.3 Baselines and Evaluation Metrics

We evaluate our PLANA3R against state-of-the-art (SOTA) planar reconstruction methods across multiple tasks, including 3D reconstruction, pose estimation, depth estimation, and plane segmentation, using diverse scene types and image pairs. These comprehensive evaluations

demonstrate our method's superior performance in both geometric accuracy (metric 3D reconstruction, depth estimation, and two-view relative pose estimation) and semantic understanding (plane segmentation). We primarily compare PLANA3R with two-view and single-image planar 3D reconstruction methods [11, 24, 28]. We also compare with the currently popular stereo metric 3D vision foundation model, MASt3R [14], which uses dense point clouds as the scene representation.

4.3.1 Metric Two-view Reconstruction

We evaluate the geometric quality of reconstructed 3D planes using Chamfer Distance and F-score on the ScanNetV2 and Matterport3D datasets. Given a pair of input images, PLANA3R predicts a collection of planar primitives, which are subsequently merged into the planar surface reconstruction using the approach described in Sec. 3.4.

We conduct extensive experiments across a wide range of scenes to evaluate the effectiveness of our method in two-view 3D reconstruction and relative pose estimation. For ScanNetV2, we follow the training and testing splits defined by NOPE-SAC [28], evaluating 4051 image pairs from 303 scenes. For Matterport3D, we evaluate 6083 image pairs from 13 challenging scenes. As shown in Tab. 1, PLANA3R achieves SOTA performance on ScanNetV2. Remarkably, despite never being trained on Matterport3D, PLANA3R outperforms prior planar reconstruction methods [11, 24, 28] that were specifically trained on this dataset, highlighting the strong zero-shot generalization capability of PLANA3R across diverse indoor environments.

We further evaluate relative camera pose estimation on ScanNetV2 and Matterport3D using the same image pairs evaluated in reconstruction. Pose accuracy is measured by the metric translation error (in meters) and rotation error (in degrees). As shown in Tab. 1, both MASt3R and our PLANA3R significantly outperform prior learning-based planar reconstruction methods [28, 11, 1] in terms of pose estimation accuracy.

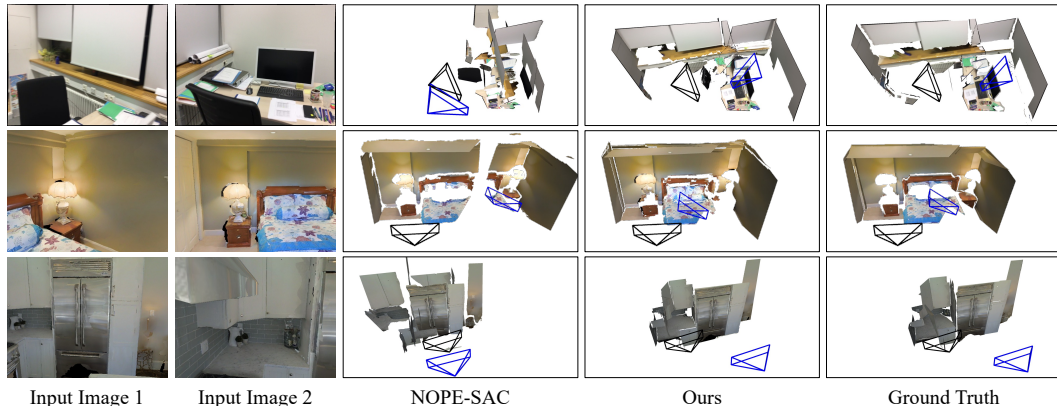| Input Image 1 | Input Image 2 | NOPE-SAC | Ours | Ground Truth |

Figure 3: Comparisons of two-view 3D planar reconstruction on the ScanNetV2 [4] (the first row) and the Matterport3D [2] (the last two rows) datasets.

4.3.2 Metric Monocular Depth Estimation

Directly rendering depth from the predicted planar primitives provides an effective means of evaluating the quality of our geometric fitting. This process does not require merging the primitives and can be performed with a single feed-forward pass. We evaluate the metric monocular depth estimation using the NYUv2-Plane dataset. NYUv2-Plane provided by [15] is a planar variant of the original NYUv2 dataset [20]. For our experiments, we use the image splits defined in [24, 15] with 654 test frames. We input two identical images into PLANA3R and use the CUDA-based differentiable planar primitive rendering module in PlanarSplatting to generate a depth map of the predicted primitives from one of the views.

Since our PLANA3R has never seen the scenes of NYUv2 during training, this dataset can well demonstrate the generalization ability of our model for out-of-domain images. As shown in Tab. 2, PLANA3R demonstrates strong zero-shot metric depth estimation performance, surpassing both prior

Table 1: Quantitative comparison of two-view planar reconstruction and relative camera pose estimation. The best results are in **bold**.

Method	Translation (m)					Rotation (°)					Chamfer↓	F-score↑
	Med.	Mean	<=1	<=0.5	<=0.1	Med.	Mean	<=30	<=15	<=5		
						ScanNetV2 dataset						
SparsePlanes [11]	0.56	0.81	73.7	44.6	–	15.46	33.38	70.5	48.7	–	–	–
PlaneFormers [1]	0.55	0.81	75.3	45.5	–	14.34	32.08	73.2	52.1	–	–	–
NOPE-SAC [28]	0.41	0.65	82	59.1	5.01	8.27	22.12	82.6	73.2	25.03	0.26	61.86
MASt3R [14]	0.11	0.19	97.65	93.98	47.37	2.17	6.67	95.04	94.08	84.37	0.21	74.92
ours	**0.07**	**0.13**	**98.62**	**97.16**	**67.91**	**2.01**	**3.16**	**99.23**	**98.89**	**93.14**	**0.11**	**92.52**
						Matterport3D dataset						
SparsePlanes [11]	0.62	1.10	67.32	40.67	3.67	7.27	22.11	84.15	73.60	36.94	0.47	48.59
NOPE-SAC [28]	0.53	0.91	73.60	47.82	4.14	2.79	13.81	89.71	87.41	69.83	0.38	54.96
MASt3R [14]	0.41	0.59	85.20	58.87	8.55	**0.98**	4.66	96.58	96.09	**92.59**	0.49	30.01
ours	**0.24**	**0.45**	**92.78**	**78.83**	**15.07**	2.00	**4.49**	**98.01**	**97.19**	89.82	**0.32**	**56.63**

learning-based planar reconstruction methods and the metric 3D vision foundation model MASt3R. These results highlight the potential of using sparse 3D planar primitives as an efficient and effective scene representation, in contrast to methods relying on heavy DPT heads [21] and dense point clouds.

Table 2: Quantitative comparison of metric monocular depth estimation on the NYUv2-Plane [20, 15] dataset. The best results are in **bold**.

Method	PlaneNet [15]	PlaneAE [40]	PlaneRCNN [16]	PlaneTR [27]	PlaneRecTR [24]	MASt3R [14]	**Ours**
Rel ↓	0.239	0.205	0.183	0.195	0.157	0.160	**0.132**
$\log_{10}$ ↓	0.124	0.097	0.076	0.095	0.073	0.065	**0.059**
RMSE ↓	0.913	0.820	0.619	0.803	0.547	0.51	**0.463**
δ_1 ↑	53.0	61.3	71.8	63.3	74.2	80.6	**86.4**
δ_2 ↑	78.3	87.2	93.1	88.2	94.2	94.7	**96.3**
δ_3 ↑	90.4	95.8	98.3	96.1	**99.0**	98.5	98.4

4.3.3 3D Plane Segmentation

The previous experiments demonstrate the geometric accuracy of our model. Here, we show that PLANA3R can perform zero-shot plane-level semantic segmentation without plane annotations. By merging predicted planar primitives, it infers semantically meaningful 3D planes. We evaluate segmentation quality using standard metrics: Variation of Information (VOI), Rand Index (RI), and Segmentation Covering (SC).

Single-view 3D Plane Segmentation   Following PlaneRCNN [16], we generate 3D plane GT labels on the Replica dataset [26] by first fitting planes to the GT mesh using RANSAC [8], and then splitting co-planar regions with different semantics into separate plane instances. A total of 498 images are sampled for single-view plane-level segmentation evaluation.

Similar to monocular depth estimation, we input two identical images into PLANA3R, then we merge the output primitives. Tab. 3 and Fig. 4 show that our PLANA3R performs better than the method trained with plane annotation in both plane segmentation and 3D reconstruction. We present more visualization results in the *supplementary materials* and conduct tests on the 7-Scenes [25] dataset.

Two-view 3D plane segmentation.   We also evaluate plane segmentation in the two-view setting. As shown in Fig. 5, our method produces results that are much better than NOPE-SAC. More results are provided in the *supplementary materials*.

Table 3: Quantitative comparison of single-view planar reconstruction on the Replica dataset [26]. The best results are in **bold**.

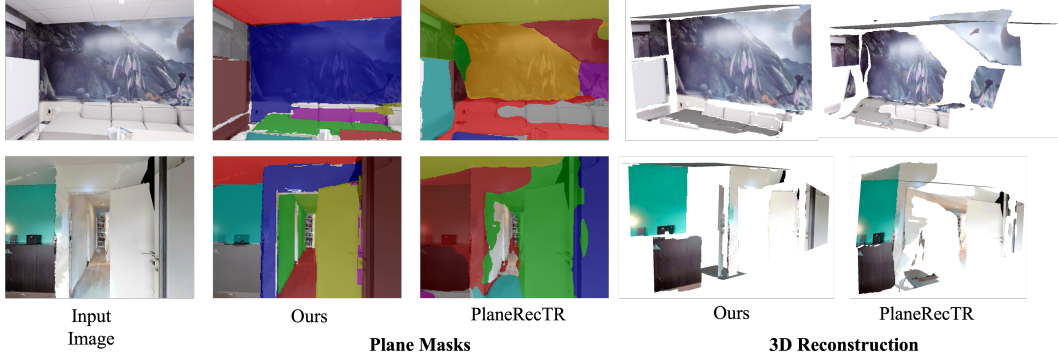| Method	Plane Segmentation			Plane Recall (depth)		Plane Recall (normal)	
	RI↑	VOI↓	SC↑	@0.1m	@0.6m	@5°	@30°
PlaneRecTR[24]	0.85	1.81	0.58	1.78	13.46	3.79	18.92
Ours	**0.89**	**1.62**	**0.63**	**7.79**	**30.74**	**28.52**	**36.31**

Figure 4: Comparisons of single-view plane segmentaion and 3D reconstruction on the Replica [26].

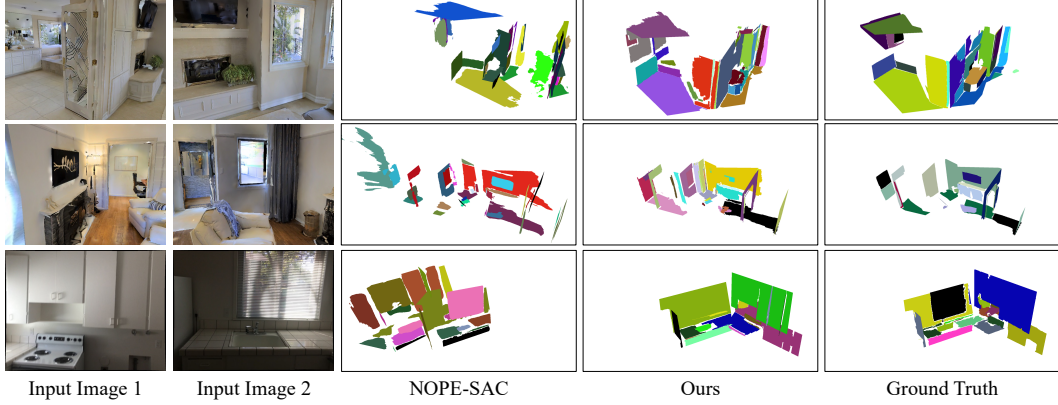Figure 5: Comparisons of two-view 3D plane segmentation on the Matterport3D [2] (the first two rows) and the ScanNetV2 [4] (the last row) datasets.

4.4 Multi-view Reconstruction with More Than Two Views

PLANA3R currently supports multi-view reconstruction in a pairwise manner, but does not support a single forward pass for inputs with three or more views. Given N input images, we construct $N - 1$ image pairs and perform $N - 1$ separate forward passes. The planar primitives predicted from each pair are then merged into a common coordinate system. To evaluate this capability, we tested PLANA3R on 50 eight-view samples, sampled every 20 frames from the ScanNetV2 dataset. For a fair comparison, we employed MASt3R also in a pairwise manner as the baseline. The quantitative results of the estimated camera trajectories are summarized in Tab. 4. We provide an example of eight-view reconstruction in Fig. 6.

4.5 Alation Study

As introduced in Sec. 3.2 and illustrated in Appendix A.4, to reduce redundancy and achieve a more compact and efficient representation, we design the HPPA module, which regulates the number of planar primitives used for rendering and merging by adjusting the gradient threshold g_{th}. In this analysis, we vary the threshold g_{th} such that, for an input resolution of 512×384, the number of generated primitives ranges from 768 (minimum, $\frac{512}{16} \times \frac{384}{16}$) to 3072 (maximum, $\frac{512}{8} \times \frac{384}{8}$).

By adjusting g_{th}, we analyze how the number of per-view primitives affects two-view 3D reconstruction and single-view depth estimation on ScanNetV2 and NYUv2, respectively. As shown in Tab. 5, using approximately half the number of high-resolution primitives achieves performance comparable to using the full high-resolution set. In contrast, relying solely on low-resolution primitives results in a significant drop in accuracy. These results demonstrate that our method can represent scenes efficiently and compactly using a highly sparse set of planar primitives.

9

Table 4: Comparison with MASt3R on multi-view RRA (Relative Rotation Accuracy) and RTA (Relative Translation Accuracy).

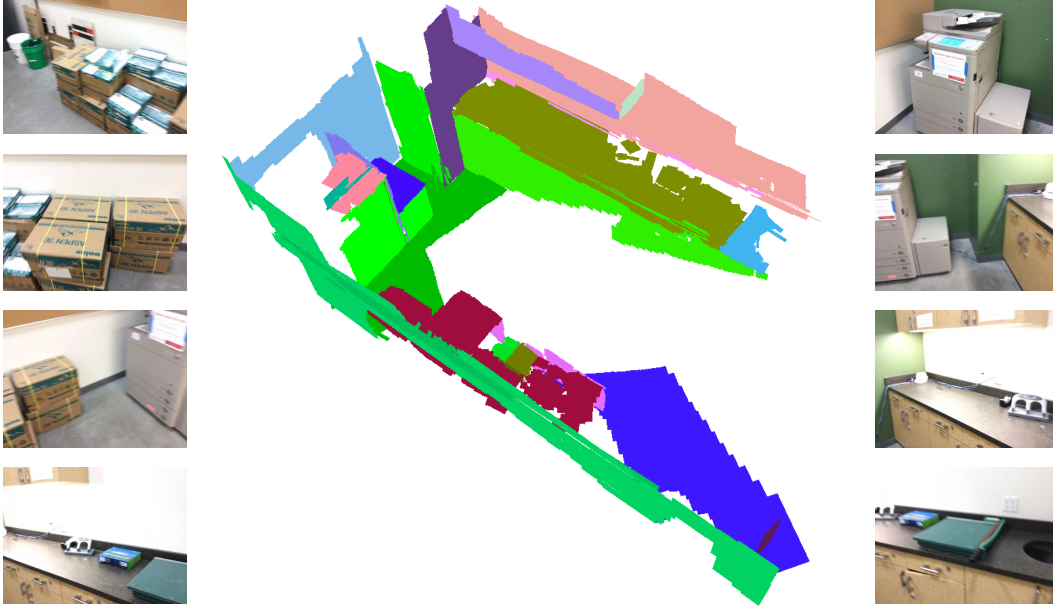| Method	RRA@5	RTA@5	RRA@10	RTA@10	RRA@15	RTA@15
Ours	0.9000	**0.3935**	**0.9985**	**0.7442**	**1.0000**	**0.8614**
MASt3R	**0.9828**	0.2657	0.9964	0.5371	**1.0000**	0.6878

Figure 6: Reconstruction example from 8 frames of a ScanNet sequence. We show the input 8 frames and planar 3D reconstruction.

Table 5: Ablation study on the gradient threshold (g_{th}). We show the relationship between the number of per-view primitives and performance.

Metrics	ScanNetV2 Reconstruction			NYUv2-Plane Depth Estimation		
	Chamfer↓	F-score↑	Avg. # primitives	RMSE↓	δ_1↑	Avg. # primitives
Ours (0)	0.10	93.10	3072	0.45	86.8	3072
Ours (0.5)	0.11	92.52	1417	0.46	86.4	1565
Ours (10)	0.11	92.32	768	0.49	85.3	768

5 Conclusion

We present PLANA3R, a zero-shot model for metric planar 3D reconstruction that exploits the geometric regularity of indoor scenes using compact 3D planar primitives. Trained without plane annotations, PLANA3R learns geometry priors from large-scale datasets through transformer-based feature extraction and differentiable planar splatting, relying only on depth and normal supervision. Extensive experiments show that PLANA3R generalizes well to out-of-domain indoor scenes and supports efficient planar reconstruction, depth estimation, relative pose estimation, and instance-level plane segmentation from unposed image pairs. We believe that our method establishes a solid foundation for large-scale learning of 3D geometry in indoor scenes and holds great potential for advancing the understanding of indoor environments, with broad applicability in emerging fields such as AR/VR and robotics.

Acknowledgments

References

[1] S. Agarwala, L. Jin, C. Rockwell, and D. F. Fouhey. Planeformers: From sparse view planes to 3d reconstruction. In *Eur. Conf. Comput. Vis.*, volume 13663, pages 192–209, 2022. doi: 10.1007/978-3-031-20062-5_12. 2, 3, 7, 8

[2] A. Chang, A. Dai, T. Funkhouser, M. Halber, M. Niessner, M. Savva, S. Song, A. Zeng, and Y. Zhang. Matterport3d: Learning from rgb-d data in indoor environments. *arXiv preprint arXiv:1709.06158*, 2017. 3, 6, 7, 9, 23

[3] Z. Chen, Q. Yan, H. Zhan, C. Cai, X. Xu, Y. Huang, W. Wang, Z. Feng, Y. Xu, and L. Liu. Planarnerf: Online learning of planar primitives with neural radiance fields. In *2025 IEEE International Conference on Robotics and Automation (ICRA)*, pages 13942–13949. IEEE, 2025. 2

[4] A. Dai, A. X. Chang, M. Savva, M. Halber, T. A. Funkhouser, and M. Nießner. Scannet: Richly-annotated 3d reconstructions of indoor scenes. In *IEEE Conf. Comput. Vis. Pattern Recog.*, pages 2432–2443, 2017. 2, 3, 6, 7, 9, 23, 24

[5] A. Dehghan, G. Baruch, Z. Chen, Y. Feigin, P. Fu, T. Gebauer, D. Kurz, T. Dimry, B. Joffe, A. Schwartz, and E. Shulman. Arkitscenes: A diverse real-world dataset for 3d indoor scene understanding using mobile RGB-D data. In *Adv. Neural Inform. Process. Syst.*, 2021. 2, 6, 24

[6] S. Dong, S. Wang, S. Liu, L. Cai, Q. Fan, J. Kannala, and Y. Yang. Reloc3r: Large-scale training of relative camera pose regression for generalizable, fast, and accurate visual localization. In *Proceedings of the Computer Vision and Pattern Recognition Conference*, pages 16739–16752, 2025. 3, 4

[7] A. Dosovitskiy, L. Beyer, A. Kolesnikov, D. Weissenborn, X. Zhai, T. Unterthiner, M. Dehghani, M. Minderer, G. Heigold, S. Gelly, J. Uszkoreit, and N. Houlsby. An image is worth 16x16 words: Transformers for image recognition at scale. In *Int. Conf. Learn. Represent.*, 2021. 2, 3, 4

[8] M. A. Fischler and R. C. Bolles. Random sample consensus: a paradigm for model fitting with applications to image analysis and automated cartography. *Communications of the ACM*, 24(6):381–395, 1981. 8

[9] Y. He, W. Zhao, S. Liu, Y. Hu, Y. Bai, Y. Wen, and Y. Liu. Alphatablets: A generic plane representation for 3d planar reconstruction from monocular videos. In *Adv. Neural Inform. Process. Syst.*, 2024. 2, 3

[10] M. Hu, W. Yin, C. Zhang, Z. Cai, X. Long, H. Chen, K. Wang, G. Yu, C. Shen, and S. Shen. Metric3d v2: A versatile monocular geometric foundation model for zero-shot metric depth and surface normal estimation. *IEEE Transactions on Pattern Analysis and Machine Intelligence*, 2024. 2, 6

[11] L. Jin, S. Qian, A. Owens, and D. F. Fouhey. Planar surface reconstruction from sparse views. In *Int. Conf. Comput. Vis.*, pages 12971–12980, 2021. doi: 10.1109/ICCV48922.2021.01275. 2, 3, 7, 8

[12] B. Ke, A. Obukhov, S. Huang, N. Metzger, R. C. Daudt, and K. Schindler. Repurposing diffusion-based image generators for monocular depth estimation. In *IEEE Conf. Comput. Vis. Pattern Recog.*, 2024. 2

[13] B. Kerbl, G. Kopanas, T. Leimkühler, and G. Drettakis. 3d gaussian splatting for real-time radiance field rendering. *ACM Trans. Graph.*, 42(4):139:1–139:14, 2023. doi: 10.1145/3592433. 4

[14] V. Leroy, Y. Cabon, and J. Revaud. Grounding image matching in 3d with mast3r. In *European Conference on Computer Vision*, pages 71–91. Springer, 2024. 2, 3, 4, 7, 8

[15] C. Liu, J. Yang, D. Ceylan, E. Yumer, and Y. Furukawa. Planenet: Piece-wise planar reconstruction from a single rgb image. In *IEEE Conf. Comput. Vis. Pattern Recog.*, pages 2579–2588, 2018. 6, 7, 8

[16] C. Liu, K. Kim, J. Gu, Y. Furukawa, and J. Kautz. Planercnn: 3d plane detection and reconstruction from a single image. In *IEEE Conf. Comput. Vis. Pattern Recog.*, pages 4450–4459, 2019. 2, 3, 8

[17] J. Liu, P. Ji, N. Bansal, C. Cai, Q. Yan, X. Huang, and Y. Xu. Planemvs: 3d plane reconstruction from multi-view stereo. In *IEEE Conf. Comput. Vis. Pattern Recog.*, pages 8655–8665, 2022. 3

[18] J. Liu, R. Yu, S. Chen, S. X. Huang, and H. Guo. Towards in-the-wild 3d plane reconstruction from a single image. In *Proceedings of the Computer Vision and Pattern Recognition Conference*, pages 27027–27037, 2025. 2

[19] I. Loshchilov and F. Hutter. Decoupled weight decay regularization. *arXiv preprint arXiv:1711.05101*, 2017. 6

[20] P. K. Nathan Silberman, Derek Hoiem and R. Fergus. Indoor segmentation and support inference from rgbd images. In *ECCV*, pages 746–760, 2012. 6, 7, 8

[21] R. Ranftl, A. Bochkovskiy, and V. Koltun. Vision transformers for dense prediction. In *Int. Conf. Comput. Vis.*, pages 12179–12188, 2021. 2, 8

[22] R. Ranftl, K. Lasinger, D. Hafner, K. Schindler, and V. Koltun. Towards robust monocular depth estimation: Mixing datasets for zero-shot cross-dataset transfer. *IEEE Trans. Pattern Anal. Mach. Intell.*, 44(3): 1623–1637, 2022. 2

[23] M. Savva, A. Kadian, O. Maksymets, Y. Zhao, E. Wijmans, B. Jain, J. Straub, J. Liu, V. Koltun, J. Malik, et al. Habitat: A platform for embodied ai research. In *IEEE Conf. Comput. Vis. Pattern Recog.*, pages 9339–9347, 2019. 2, 6, 21, 24

[24] J. Shi, S. Zhi, and K. Xu. Planerectr: Unified query learning for 3d plane recovery from a single view. In *Int. Conf. Comput. Vis.*, pages 9343–9352, 2023. 2, 3, 7, 8

[25] J. Shotton, B. Glocker, C. Zach, S. Izadi, A. Criminisi, and A. Fitzgibbon. Scene coordinate regression forests for camera relocalization in rgb-d images. In *Int. Conf. Comput. Vis.*, pages 2930–2937, 2013. 6, 8, 21, 22

[26] J. Straub, T. Whelan, L. Ma, Y. Chen, E. Wijmans, S. Green, J. J. Engel, R. Mur-Artal, C. Ren, S. Verma, A. Clarkson, M. Yan, B. Budge, Y. Yan, X. Pan, J. Yon, Y. Zou, K. Leon, N. Carter, J. Briales, T. Gillingham, E. Mueggler, L. Pesqueira, M. Savva, D. Batra, H. M. Strasdat, R. D. Nardi, M. Goesele, S. Lovegrove, and R. Newcombe. The Replica dataset: A digital replica of indoor spaces. *arXiv preprint arXiv:1906.05797*, 2019. 6, 8, 9, 22

[27] B. Tan, N. Xue, S. Bai, T. Wu, and G. Xia. Planetr: Structure-guided transformers for 3d plane recovery. In *Int. Conf. Comput. Vis.*, pages 4166–4175, 2021. 2, 3, 8

[28] B. Tan, N. Xue, T. Wu, and G. Xia. NOPE-SAC: neural one-plane RANSAC for sparse-view planar 3d reconstruction. *IEEE Trans. Pattern Anal. Mach. Intell.*, 45(12):15233–15248, 2023. doi: 10.1109/TPAMI. 2023.3314745. 2, 3, 7, 8

[29] B. Tan, R. Yu, Y. Shen, and N. Xue. Planarsplatting: Accurate planar surface reconstruction in 3 minutes. *arXiv preprint arXiv:2412.03451*, 2024. 2, 3, 4, 5

[30] Z. Tang, Y. Fan, D. Wang, H. Xu, R. Ranjan, A. Schwing, and Z. Yan. Mv-dust3r+: Single-stage scene reconstruction from sparse views in 2 seconds. In *Proceedings of the Computer Vision and Pattern Recognition Conference*, pages 5283–5293, 2025. 2, 3

[31] H. Wang and L. Agapito. 3d reconstruction with spatial memory. In *2025 International Conference on 3D Vision (3DV)*, pages 78–89. IEEE, 2025. 2, 3

[32] J. Wang, M. Chen, N. Karaev, A. Vedaldi, C. Rupprecht, and D. Novotny. Vggt: Visual geometry grounded transformer. In *Proceedings of the Computer Vision and Pattern Recognition Conference*, pages 5294–5306, 2025. 2, 3

[33] S. Wang, V. Leroy, Y. Cabon, B. Chidlovskii, and J. Revaud. Dust3r: Geometric 3d vision made easy. In *IEEE Conf. Comput. Vis. Pattern Recog.*, pages 20697–20709, 2024. 2, 3, 4, 21

[34] J. Watson, F. Aleotti, M. Sayed, Z. Qureshi, O. M. Aodha, G. J. Brostow, M. Firman, and S. Vicente. Airplanes: Accurate plane estimation via 3d-consistent embeddings. In *IEEE Conf. Comput. Vis. Pattern Recog.*, pages 5270–5280, 2024. 3

[35] P. Weinzaepfel, V. Leroy, T. Lucas, R. Brégier, Y. Cabon, V. Arora, L. Antsfeld, B. Chidlovskii, G. Csurka, and J. Revaud. Croco: Self-supervised pre-training for 3d vision tasks by cross-view completion. In *Adv. Neural Inform. Process. Syst.*, 2022. 4

[36] Y. Xie, M. Gadelha, F. Yang, X. Zhou, and H. Jiang. Planarrecon: Realtime 3d plane detection and reconstruction from posed monocular videos. In *IEEE Conf. Comput. Vis. Pattern Recog.*, pages 6209–6218, 2022. 2, 3

[37] J. Yang, A. Sax, K. J. Liang, M. Henaff, H. Tang, A. Cao, J. Chai, F. Meier, and M. Feiszli. Fast3r: Towards 3d reconstruction of 1000+ images in one forward pass. In *Proceedings of the Computer Vision and Pattern Recognition Conference*, pages 21924–21935, 2025. 2, 3

[38] H. Ye, Y. Liu, Y. Liu, and S. Shen. Neuralplane: Structured 3d reconstruction in planar primitives with neural fields. In *Int. Conf. Learn. Represent.*, 2025. 2, 3

[39] C. Yeshwanth, Y. Liu, M. Nießner, and A. Dai. Scannet++: A high-fidelity dataset of 3d indoor scenes. In *Int. Conf. Comput. Vis.*, pages 12–22, 2023. 2, 6, 24

[40] Z. Yu, J. Zheng, D. Lian, Z. Zhou, and S. Gao. Single-image piece-wise planar 3d reconstruction via associative embedding. In *IEEE Conf. Comput. Vis. Pattern Recog.*, pages 1029–1037, 2019. 2, 3, 8

[41] S. Zhang, J. Wang, Y. Xu, N. Xue, C. Rupprecht, X. Zhou, Y. Shen, and G. Wetzstein. Flare: Feed-forward geometry, appearance and camera estimation from uncalibrated sparse views. In *Proceedings of the Computer Vision and Pattern Recognition Conference*, pages 21936–21947, 2025. 2, 3

[42] W. Zhao, J. Liu, S. Zhang, Y. Li, S. Chen, S. X. Huang, Y.-J. Liu, and H. Guo. Monoplane: exploiting monocular geometric cues for generalizable 3d plane reconstruction. In *2024 IEEE/RSJ International Conference on Intelligent Robots and Systems (IROS)*, pages 8481–8488. IEEE, 2024. 2

NeurIPS Paper Checklist

1. **Claims**

   Question: Do the main claims made in the abstract and introduction accurately reflect the paper's contributions and scope?

   Answer: [Yes]

   Justification: See our Abstract and Sec. 1

   Guidelines:

   - The answer NA means that the abstract and introduction do not include the claims made in the paper.
   - The abstract and/or introduction should clearly state the claims made, including the contributions made in the paper and important assumptions and limitations. A No or NA answer to this question will not be perceived well by the reviewers.
   - The claims made should match theoretical and experimental results, and reflect how much the results can be expected to generalize to other settings.
   - It is fine to include aspirational goals as motivation as long as it is clear that these goals are not attained by the paper.

2. **Limitations**

   Question: Does the paper discuss the limitations of the work performed by the authors?

   Answer: [Yes]

   Justification: See Appendix A.5.

   Guidelines:

   - The answer NA means that the paper has no limitation while the answer No means that the paper has limitations, but those are not discussed in the paper.
   - The authors are encouraged to create a separate "Limitations" section in their paper.
   - The paper should point out any strong assumptions and how robust the results are to violations of these assumptions (e.g., independence assumptions, noiseless settings, model well-specification, asymptotic approximations only holding locally). The authors should reflect on how these assumptions might be violated in practice and what the implications would be.
   - The authors should reflect on the scope of the claims made, e.g., if the approach was only tested on a few datasets or with a few runs. In general, empirical results often depend on implicit assumptions, which should be articulated.
   - The authors should reflect on the factors that influence the performance of the approach. For example, a facial recognition algorithm may perform poorly when image resolution is low or images are taken in low lighting. Or a speech-to-text system might not be used reliably to provide closed captions for online lectures because it fails to handle technical jargon.
   - The authors should discuss the computational efficiency of the proposed algorithms and how they scale with dataset size.
   - If applicable, the authors should discuss possible limitations of their approach to address problems of privacy and fairness.
   - While the authors might fear that complete honesty about limitations might be used by reviewers as grounds for rejection, a worse outcome might be that reviewers discover limitations that aren't acknowledged in the paper. The authors should use their best judgment and recognize that individual actions in favor of transparency play an important role in developing norms that preserve the integrity of the community. Reviewers will be specifically instructed to not penalize honesty concerning limitations.

3. **Theory assumptions and proofs**

   Question: For each theoretical result, does the paper provide the full set of assumptions and a complete (and correct) proof?

   Answer: [NA]

Justification: This paper does not include theoretical results.

Guidelines:

- The answer NA means that the paper does not include theoretical results.
- All the theorems, formulas, and proofs in the paper should be numbered and cross-referenced.
- All assumptions should be clearly stated or referenced in the statement of any theorems.
- The proofs can either appear in the main paper or the supplemental material, but if they appear in the supplemental material, the authors are encouraged to provide a short proof sketch to provide intuition.
- Inversely, any informal proof provided in the core of the paper should be complemented by formal proofs provided in appendix or supplemental material.
- Theorems and Lemmas that the proof relies upon should be properly referenced.

4. **Experimental result reproducibility**

Question: Does the paper fully disclose all the information needed to reproduce the main experimental results of the paper to the extent that it affects the main claims and/or conclusions of the paper (regardless of whether the code and data are provided or not)?

Answer: [Yes]

Justification: We have provided detailed descriptions of our network architecture, the training and testing datasets, the evaluation protocols, and the implementation details of our experiments. Comparisons with existing methods are conducted using their official open-source implementations.

Guidelines:

- The answer NA means that the paper does not include experiments.
- If the paper includes experiments, a No answer to this question will not be perceived well by the reviewers: Making the paper reproducible is important, regardless of whether the code and data are provided or not.
- If the contribution is a dataset and/or model, the authors should describe the steps taken to make their results reproducible or verifiable.
- Depending on the contribution, reproducibility can be accomplished in various ways. For example, if the contribution is a novel architecture, describing the architecture fully might suffice, or if the contribution is a specific model and empirical evaluation, it may be necessary to either make it possible for others to replicate the model with the same dataset, or provide access to the model. In general. releasing code and data is often one good way to accomplish this, but reproducibility can also be provided via detailed instructions for how to replicate the results, access to a hosted model (e.g., in the case of a large language model), releasing of a model checkpoint, or other means that are appropriate to the research performed.
- While NeurIPS does not require releasing code, the conference does require all submissions to provide some reasonable avenue for reproducibility, which may depend on the nature of the contribution. For example
  (a) If the contribution is primarily a new algorithm, the paper should make it clear how to reproduce that algorithm.
  (b) If the contribution is primarily a new model architecture, the paper should describe the architecture clearly and fully.
  (c) If the contribution is a new model (e.g., a large language model), then there should either be a way to access this model for reproducing the results or a way to reproduce the model (e.g., with an open-source dataset or instructions for how to construct the dataset).
  (d) We recognize that reproducibility may be tricky in some cases, in which case authors are welcome to describe the particular way they provide for reproducibility. In the case of closed-source models, it may be that access to the model is limited in some way (e.g., to registered users), but it should be possible for other researchers to have some path to reproducing or verifying the results.

5. **Open access to data and code**

Question: Does the paper provide open access to the data and code, with sufficient instructions to faithfully reproduce the main experimental results, as described in supplemental material?

Answer: [Yes]

Justification: All the datasets used in this paper are public. The code is publicly available on our project page at `https://lck666666.github.io/plana3r/`.

Guidelines:

- The answer NA means that paper does not include experiments requiring code.
- Please see the NeurIPS code and data submission guidelines (`https://nips.cc/public/guides/CodeSubmissionPolicy`) for more details.
- While we encourage the release of code and data, we understand that this might not be possible, so "No" is an acceptable answer. Papers cannot be rejected simply for not including code, unless this is central to the contribution (e.g., for a new open-source benchmark).
- The instructions should contain the exact command and environment needed to run to reproduce the results. See the NeurIPS code and data submission guidelines (`https://nips.cc/public/guides/CodeSubmissionPolicy`) for more details.
- The authors should provide instructions on data access and preparation, including how to access the raw data, preprocessed data, intermediate data, and generated data, etc.
- The authors should provide scripts to reproduce all experimental results for the new proposed method and baselines. If only a subset of experiments are reproducible, they should state which ones are omitted from the script and why.
- At submission time, to preserve anonymity, the authors should release anonymized versions (if applicable).
- Providing as much information as possible in supplemental material (appended to the paper) is recommended, but including URLs to data and code is permitted.

6. **Experimental setting/details**

Question: Does the paper specify all the training and test details (e.g., data splits, hyperparameters, how they were chosen, type of optimizer, etc.) necessary to understand the results?

Answer: [Yes]

Justification: Please check Sec. 4.1 and Appendix A.2.

Guidelines:

- The answer NA means that the paper does not include experiments.
- The experimental setting should be presented in the core of the paper to a level of detail that is necessary to appreciate the results and make sense of them.
- The full details can be provided either with the code, in appendix, or as supplemental material.

7. **Experiment statistical significance**

Question: Does the paper report error bars suitably and correctly defined or other appropriate information about the statistical significance of the experiments?

Answer: [Yes]

Justification: The statistical significance of the experiments is provided in the paper.

Guidelines:

- The answer NA means that the paper does not include experiments.
- The authors should answer "Yes" if the results are accompanied by error bars, confidence intervals, or statistical significance tests, at least for the experiments that support the main claims of the paper.
- The factors of variability that the error bars are capturing should be clearly stated (for example, train/test split, initialization, random drawing of some parameter, or overall run with given experimental conditions).

- The method for calculating the error bars should be explained (closed form formula, call to a library function, bootstrap, etc.)
- The assumptions made should be given (e.g., Normally distributed errors).
- It should be clear whether the error bar is the standard deviation or the standard error of the mean.
- It is OK to report 1-sigma error bars, but one should state it. The authors should preferably report a 2-sigma error bar than state that they have a 96% CI, if the hypothesis of Normality of errors is not verified.
- For asymmetric distributions, the authors should be careful not to show in tables or figures symmetric error bars that would yield results that are out of range (e.g. negative error rates).
- If error bars are reported in tables or plots, The authors should explain in the text how they were calculated and reference the corresponding figures or tables in the text.

8. **Experiments compute resources**

   Question: For each experiment, does the paper provide sufficient information on the computer resources (type of compute workers, memory, time of execution) needed to reproduce the experiments?

   Answer: [Yes]

   Justification: Please check Sec. 4.1 and Appendix A.3.

   Guidelines:
   - The answer NA means that the paper does not include experiments.
   - The paper should indicate the type of compute workers CPU or GPU, internal cluster, or cloud provider, including relevant memory and storage.
   - The paper should provide the amount of compute required for each of the individual experimental runs as well as estimate the total compute.
   - The paper should disclose whether the full research project required more compute than the experiments reported in the paper (e.g., preliminary or failed experiments that didn't make it into the paper).

9. **Code of ethics**

   Question: Does the research conducted in the paper conform, in every respect, with the NeurIPS Code of Ethics https://neurips.cc/public/EthicsGuidelines?

   Answer: [Yes]

   Justification: The research conducted in the paper conforms with the NeurIPS Code of ethics.

   Guidelines:
   - The answer NA means that the authors have not reviewed the NeurIPS Code of Ethics.
   - If the authors answer No, they should explain the special circumstances that require a deviation from the Code of Ethics.
   - The authors should make sure to preserve anonymity (e.g., if there is a special consideration due to laws or regulations in their jurisdiction).

10. **Broader impacts**

    Question: Does the paper discuss both potential positive societal impacts and negative societal impacts of the work performed?

    Answer: [Yes]

    Justification: The paper has discussed both the potential positive societal impacts and negative societal impacts of the work performed.

    Guidelines:
    - The answer NA means that there is no societal impact of the work performed.
    - If the authors answer NA or No, they should explain why their work has no societal impact or why the paper does not address societal impact.

- Examples of negative societal impacts include potential malicious or unintended uses (e.g., disinformation, generating fake profiles, surveillance), fairness considerations (e.g., deployment of technologies that could make decisions that unfairly impact specific groups), privacy considerations, and security considerations.
- The conference expects that many papers will be foundational research and not tied to particular applications, let alone deployments. However, if there is a direct path to any negative applications, the authors should point it out. For example, it is legitimate to point out that an improvement in the quality of generative models could be used to generate deepfakes for disinformation. On the other hand, it is not needed to point out that a generic algorithm for optimizing neural networks could enable people to train models that generate Deepfakes faster.
- The authors should consider possible harms that could arise when the technology is being used as intended and functioning correctly, harms that could arise when the technology is being used as intended but gives incorrect results, and harms following from (intentional or unintentional) misuse of the technology.
- If there are negative societal impacts, the authors could also discuss possible mitigation strategies (e.g., gated release of models, providing defenses in addition to attacks, mechanisms for monitoring misuse, mechanisms to monitor how a system learns from feedback over time, improving the efficiency and accessibility of ML).

11. **Safeguards**

Question: Does the paper describe safeguards that have been put in place for responsible release of data or models that have a high risk for misuse (e.g., pretrained language models, image generators, or scraped datasets)?

Answer: [NA]

Justification: Our model was trained on publicly available datasets. We did not observe any risk for misuse.

Guidelines:

- The answer NA means that the paper poses no such risks.
- Released models that have a high risk for misuse or dual-use should be released with necessary safeguards to allow for controlled use of the model, for example by requiring that users adhere to usage guidelines or restrictions to access the model or implementing safety filters.
- Datasets that have been scraped from the Internet could pose safety risks. The authors should describe how they avoided releasing unsafe images.
- We recognize that providing effective safeguards is challenging, and many papers do not require this, but we encourage authors to take this into account and make a best faith effort.

12. **Licenses for existing assets**

Question: Are the creators or original owners of assets (e.g., code, data, models), used in the paper, properly credited and are the license and terms of use explicitly mentioned and properly respected?

Answer: [Yes]

Justification: We have correctly cited the references regarding to the public datasets and models. Our usage did not violate the license and terms of use of those assets.

Guidelines:

- The answer NA means that the paper does not use existing assets.
- The authors should cite the original paper that produced the code package or dataset.
- The authors should state which version of the asset is used and, if possible, include a URL.
- The name of the license (e.g., CC-BY 4.0) should be included for each asset.
- For scraped data from a particular source (e.g., website), the copyright and terms of service of that source should be provided.

- If assets are released, the license, copyright information, and terms of use in the package should be provided. For popular datasets, paperswithcode.com/datasets has curated licenses for some datasets. Their licensing guide can help determine the license of a dataset.
- For existing datasets that are re-packaged, both the original license and the license of the derived asset (if it has changed) should be provided.
- If this information is not available online, the authors are encouraged to reach out to the asset's creators.

13. **New assets**

    Question: Are new assets introduced in the paper well documented and is the documentation provided alongside the assets?

    Answer: [Yes]

    Justification: All code and models for our proposed method are currently well-documented in a private repository. Upon public release, we will provide comprehensive documentation to support replication and usage, along with the associated assets.

    Guidelines:

    - The answer NA means that the paper does not release new assets.
    - Researchers should communicate the details of the dataset/code/model as part of their submissions via structured templates. This includes details about training, license, limitations, etc.
    - The paper should discuss whether and how consent was obtained from people whose asset is used.
    - At submission time, remember to anonymize your assets (if applicable). You can either create an anonymized URL or include an anonymized zip file.

14. **Crowdsourcing and research with human subjects**

    Question: For crowdsourcing experiments and research with human subjects, does the paper include the full text of instructions given to participants and screenshots, if applicable, as well as details about compensation (if any)?

    Answer: [NA]

    Justification: Our paper does not involve crowdsourcing nor research with human subjects.

    Guidelines:

    - The answer NA means that the paper does not involve crowdsourcing nor research with human subjects.
    - Including this information in the supplemental material is fine, but if the main contribution of the paper involves human subjects, then as much detail as possible should be included in the main paper.
    - According to the NeurIPS Code of Ethics, workers involved in data collection, curation, or other labor should be paid at least the minimum wage in the country of the data collector.

15. **Institutional review board (IRB) approvals or equivalent for research with human subjects**

    Question: Does the paper describe potential risks incurred by study participants, whether such risks were disclosed to the subjects, and whether Institutional Review Board (IRB) approvals (or an equivalent approval/review based on the requirements of your country or institution) were obtained?

    Answer: [NA]

    Justification: This paper does not involve crowdsourcing nor research with human subjects.

    Guidelines:

    - The answer NA means that the paper does not involve crowdsourcing nor research with human subjects.

- Depending on the country in which research is conducted, IRB approval (or equivalent) may be required for any human subjects research. If you obtained IRB approval, you should clearly state this in the paper.
- We recognize that the procedures for this may vary significantly between institutions and locations, and we expect authors to adhere to the NeurIPS Code of Ethics and the guidelines for their institution.
- For initial submissions, do not include any information that would break anonymity (if applicable), such as the institution conducting the review.

16. **Declaration of LLM usage**

Question: Does the paper describe the usage of LLMs if it is an important, original, or non-standard component of the core methods in this research? Note that if the LLM is used only for writing, editing, or formatting purposes and does not impact the core methodology, scientific rigorousness, or originality of the research, declaration is not required.

Answer: [NA]

Justification: LLM is used only for writing, editing, or formatting purposes in this paper.

Guidelines:

- The answer NA means that the core method development in this research does not involve LLMs as any important, original, or non-standard components.
- Please refer to our LLM policy (https://neurips.cc/Conferences/2025/LLM) for what should or should not be described.

A Technical Appendices and Supplementary Material

This appendix provides more details and results of our PLANA3R.

A.1 Extra Results

We present additional visualization results here.

Single-view 3D Reconstruction and Plane Segmentation. To further demonstrate the zero-shot generalization capability of our method in out-of-domain scenes, we evaluate single-view reconstruction and planar segmentation on the 7-Scenes dataset [25]. Although the 7-Scenes dataset is a widely used indoor dataset and is very suitable for out-of-domain evaluation, it does not provide official plane segmentation masks. We attempted to generate them via mesh synthesis but found it challenging to obtain high-quality ground truth labels. Therefore, we present the visualization results. As shown in Fig. 7, our method achieves much better planar segmentation and reconstruction performance than PlaneRecTR.

Two-view 3D Reconstruction and Plane Segmentation. We provide more results in Fig. 8 to show that PLANA3R achieves much better performance than NOPE-SAC.

A.2 Implementation Details

Data Augmentation. PLANA3R is trained on a combination of four public indoor datasets as shown in Tab. 7. Due to the low visual quality of rendered RGB images in Habitat [23], we include only a small subset of synthetic images during training and primarily rely on real-world data. Following the training strategy of DUSt3R [33], we apply color jittering and construct symmetric image pairs, (I^1, I^2) and (I^2, I^1), for data augmentation. In our training set (totally around 4M image pairs), we include approximately 0.57M image pairs with no overlap, while the remaining 3.43M pairs are randomly sampled from nearby frames (mainly within the next 10 frames). We observed that incorporating the 0.57M non-overlapping pairs helps the model learn strong geometric priors, enabling it to infer relative pose and scene geometry even when the two views have little or no overlap, as shown in Fig. 8.

Table 6: Results on ScanNetV2 and MP3D (w/o Ext. Data means training without 0.57M non-overlapping image pairs).

Overlap	Training Data	Translation Med. (m)↓	Translation Mean (m)↓	≤0.2m↑	Rotation Med. (°)↓	Rotation Mean (°)↓	≤10° ↑
ScanNetV2							
Easy (>50%)	Full	0.05	0.07	97.40	1.53	1.80	99.72
	w/o Ext. Data	0.05	0.09	95.73	1.77	2.77	99.16
Medium (15–50%)	Full	0.06	0.10	93.56	2.02	2.68	98.88
	w/o Ext. Data	0.07	0.15	89.68	2.25	4.24	97.60
Hard (<15%)	Full	0.12	0.26	71.98	2.68	5.53	95.67
	w/o Ext. Data	0.15	0.41	63.03	3.46	10.35	88.30
Very Hard (non-overlap)	Full	0.19	0.37	51.26	2.87	7.45	94.12
	w/o Ext. Data	0.23	0.53	46.22	4.16	16.64	79.83
All	Full	0.07	0.13	89.16	2.01	3.16	98.30
	w/o Ext. Data	0.07	0.20	84.60	2.31	5.38	95.68
MP3D							
Easy (>50%)	Full	0.20	0.33	49.72	1.65	2.37	99.15
	w/o Ext. Data	0.23	0.49	44.84	1.92	4.29	97.08
Medium (15–50%)	Full	0.25	0.45	37.55	2.19	4.46	96.41
	w/o Ext. Data	0.29	0.66	36.75	2.41	7.67	91.81
Hard (<15%)	Full	0.46	0.82	17.35	2.96	11.12	85.97
	w/o Ext. Data	0.59	1.03	14.26	3.17	17.84	79.52
Very Hard (non-overlap)	Full	0.82	1.11	5.63	3.00	12.37	85.28
	w/o Ext. Data	0.85	1.11	5.19	2.98	18.84	79.65
All	Full	0.24	0.45	40.16	2.00	4.49	96.12
	w/o Ext. Data	0.29	0.64	37.14	2.24	7.62	92.37

Input Image	Ours	PlaneRecTR	Ours	PlaneRecTR
	Plane Masks		**3D Reconstruction**	

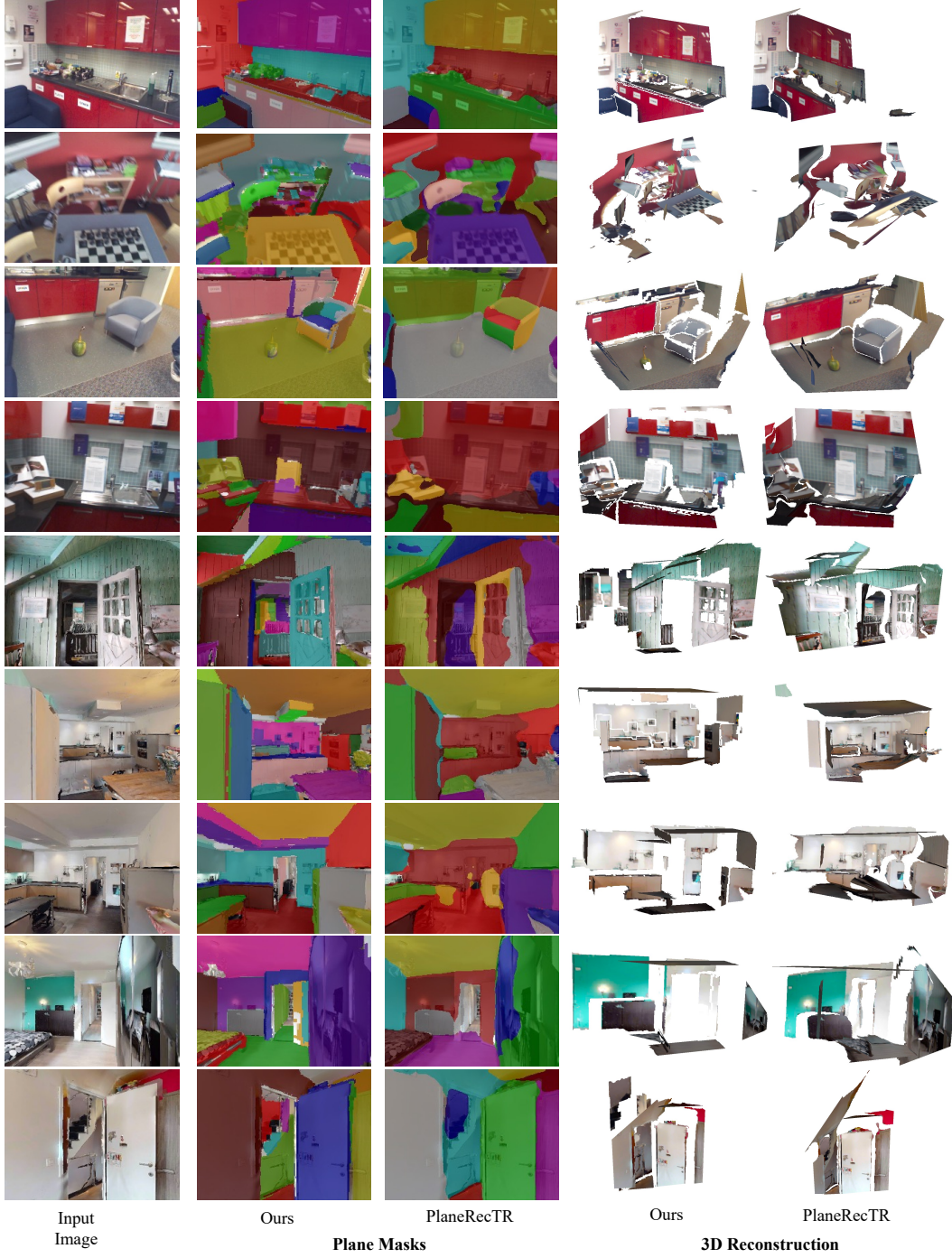Figure 7: Supplement comparisons of single-view plane segmentaion and 3D reconstruction on the 7-Scenes [25] (the first four rows) and Replica [26] (the last four rows).

Performance Analysis on Pair's Overlap   We also conduct an additional ablation study to evaluate the impact of incorporating the 0.57M non-overlapping image pairs on model performance during training. In addition, we analyze how the overlap ratio affects performance. Specifically, we define the overlap ratio as the maximum percentage of pixels in one image (either the first or the second) that have direct correspondences in the other. We provide a quantitative analysis to show the impact of including the 0.57M non-overlapping image pairs in Tab. 6.

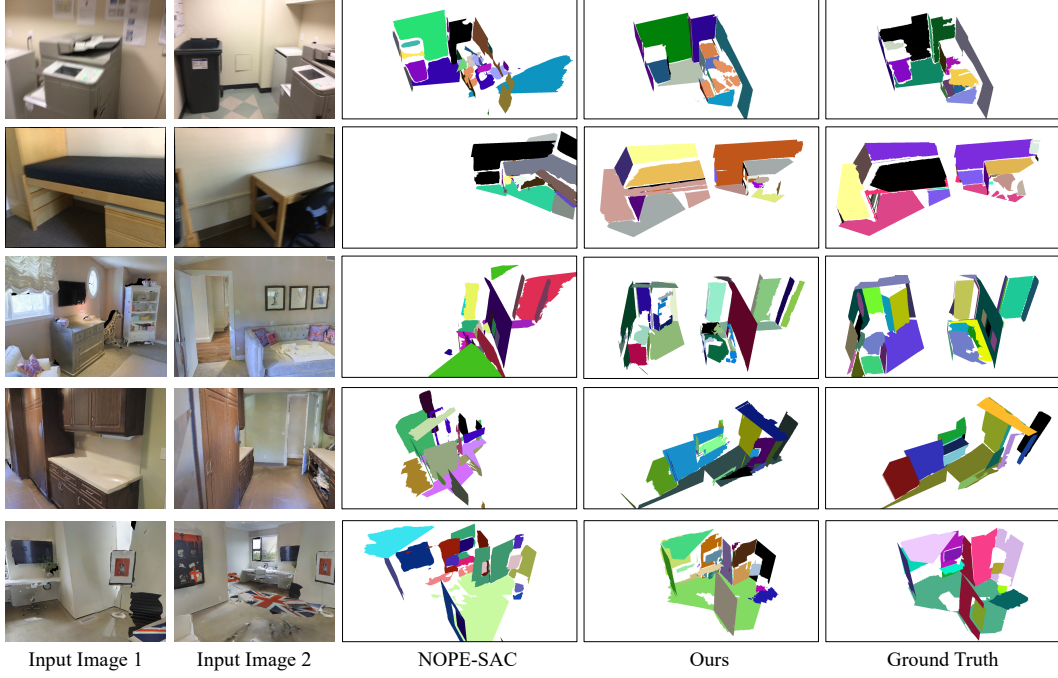| Input Image 1 | Input Image 2 | NOPE-SAC | Ours | Ground Truth |

Figure 8: Supplement comparisons of two-view 3D plane segmentaion on the ScanNetV2 [4] (the first two rows) and Matterport3D [2] (the last three rows).

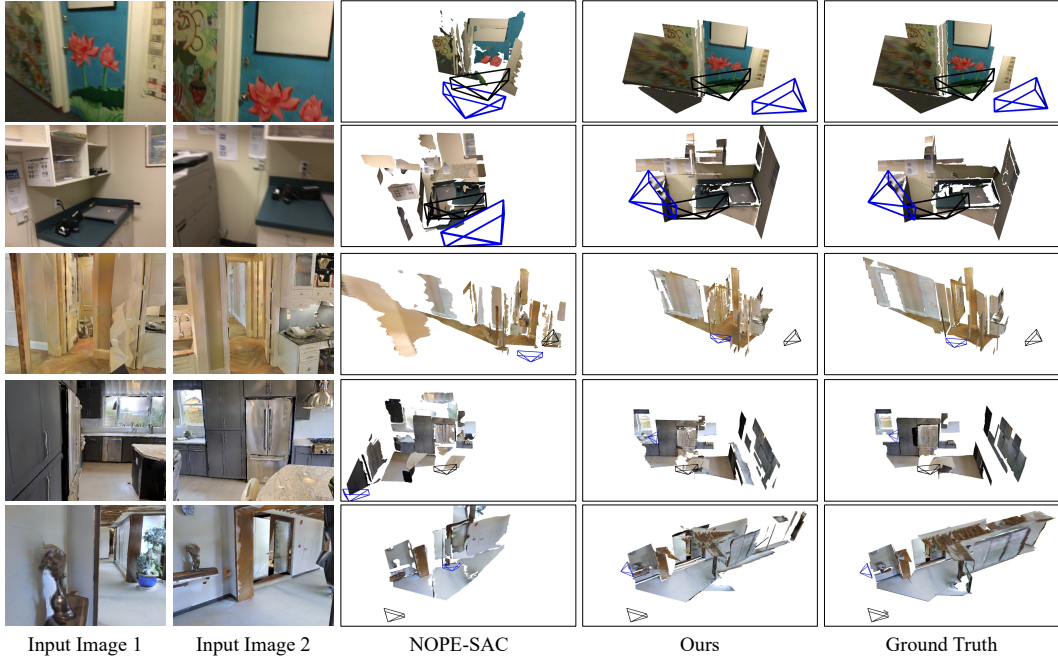| Input Image 1 | Input Image 2 | NOPE-SAC | Ours | Ground Truth |

Figure 9: Supplement comparisons of two-view 3D plane reconstruction on the ScanNetV2 [4] (the first two rows) and Matterport3D [2] (the last three rows).

As shown in Fig. 11 and Tab. 6, including these non-overlapping pairs improves the model's overall performance. Furthermore, we observe that as the overlap ratio in the test set decreases, the model's accuracy consistently degrades.
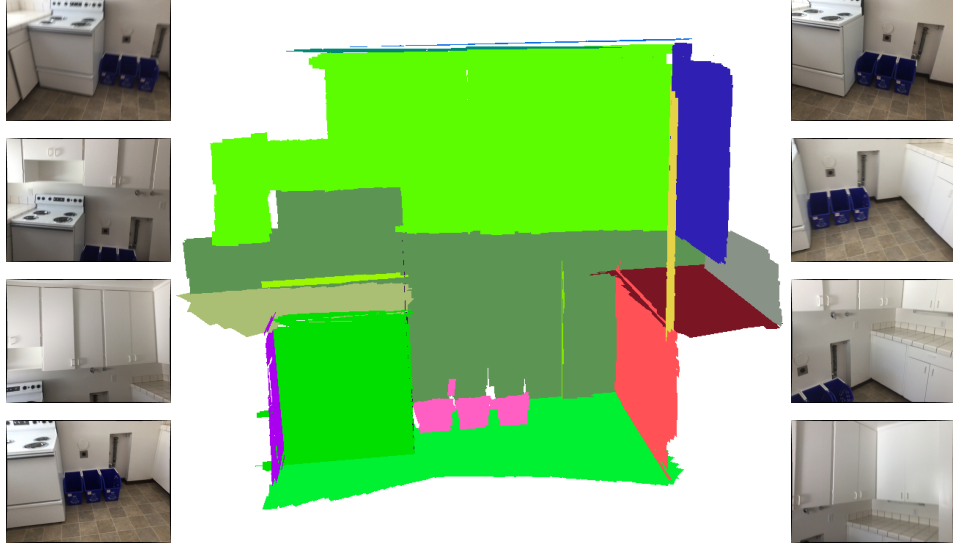
Figure 10: Reconstruction example from 8 frames of a ScanNet sequence. We show the input 8 frames and planar 3D reconstruction.
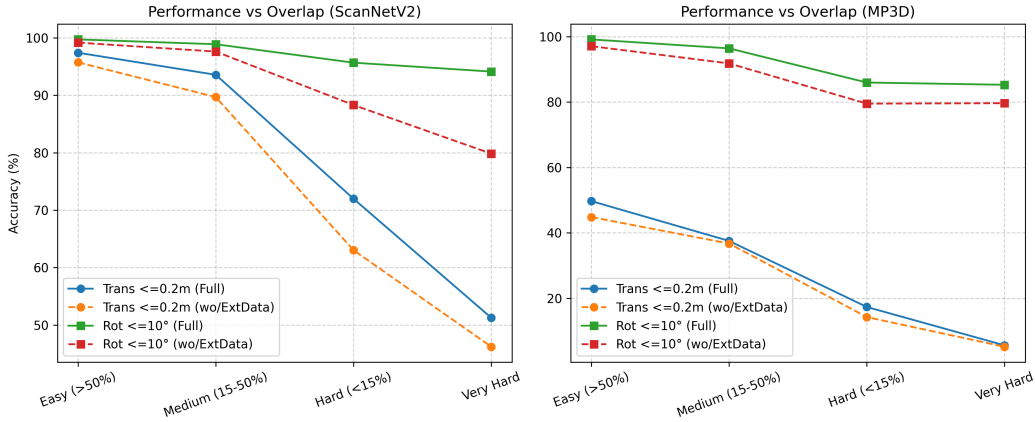

Figure 11: Test-time performance versus overlap degree.

Plane merge. Our PLANA3R predicts a set of 3D planar primitives from the inputs. To further achieve instances of 3D planes, we merge the predicted primitives according to their spatial connectivity and geometric similarity. In detail, we greedily merge adjacent planar primitives that meet the merging thresholds (projection distance ≤ 0.1m and normal angle difference ≤ 25 degrees) to obtain the final 3D plane instances.

Table 7: Training data and sample sizes for PLANA3R.

Datasets	Type	N Pairs
ScanNetV2 [4]	Indoor/Real	610K
ScanNet++ [39]	Indoor/Real	810K
ARKitScenes [5]	Indoor/Real	2400K
Habitat [23]	Indoor/Synthetic	120k

Hyperparameters. For our final model used for evaluation, we set the loss weights $\alpha_1 = 5$, $\alpha_2 = 5$, $\alpha_3 = 20$ in Eq. (3). We set the loss weights $\beta_1 = 1$, $\beta_2 = 1$, $\beta_3 = 2$ in Eq. (4). We set the loss weights $\gamma_1 = 10$, $\gamma_2 = 10$, $\gamma_3 = 1$ in Eq. (5). We observed that increasing the weights of the patch

24

loss facilitates faster convergence during the training process. This improvement can be attributed to the fact that more accurate primitive depth estimation ensures proper differentiable rendering and gradient propagation for a larger number of primitives. This occurs because primitives with very incorrect spatial positions or orientations lie outside the camera's viewing frustum, preventing them from being rendered.

A.3   Runtime Analysis

We evaluate the inference runtime of our PLANA3R using an NVIDIA RTX 3090 GPU. On average, a single feed-forward pass takes 70 ms for predicting planar primitives and relative camera pose. Efficient CUDA-based planar primitive rendering achieves a rate of 1000 fps.

A.4   Planar Primitive and Primitive Selection

We show the representation of a 3D planar primitive in Fig. 12 (a). We further explain the module of primitive selection in Fig. 12 (b).
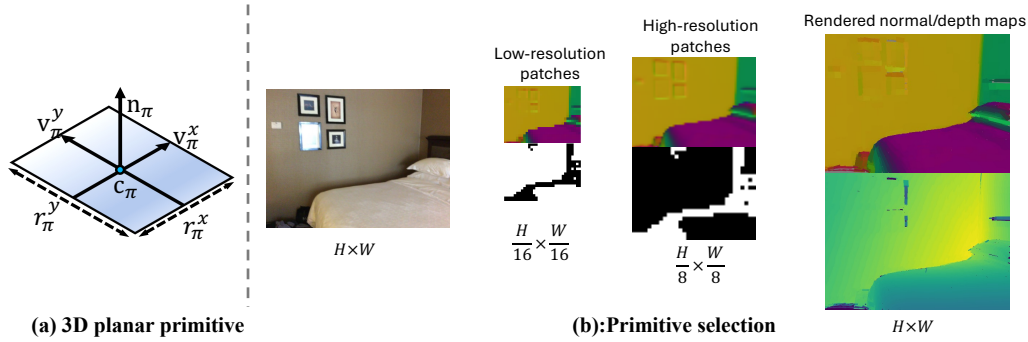

(a) 3D planar primitive   **(b):Primitive selection**

Figure 12: (a) A 3D planar primitive using learnable shape parameters. V_π^x and V_π^y are the positive direction of the X-axis and Y-axis, respectively. (b) We compute the gradient magnitude for each pixel in $\frac{H}{16} \times \frac{W}{16}$ low-resolution predicted normal patches $\mathbf{N}_{\text{low}}^{\text{patch}}$. To combine the low- and high-resolution primitives, we use binary masks (with **white** indicating valid regions) to merge only the valid patches from both resolutions, rather than directly using all predicted primitives.

A.5   Limitations

We conduct extensive experiments on five test sets. However, when evaluating plane segmentation, the absence of high-quality out-of-domain datasets with reliable plane-level annotations poses a challenge. Although we attempt to generate pseudo-labels, their limited accuracy restricts us to primarily qualitative evaluation. While this represents a limitation in our current analysis, it also highlights the urgent need for better benchmarks in this field. Despite this, the visual results demonstrate the strong potential of our zero-shot method in producing accurate pseudo-plane annotations.

A.6   Social Impacts

Positive Social Impact.   Our zero-shot, pose-free planar primitive framework significantly broadens the applicability of planar 3D reconstruction. Due to its lightweight design and lack of reliance on camera pose or plane annotations, our model can be easily deployed in real-world applications such as AR/VR and robotics, enhancing 3D scene understanding and perception in indoor environments.

Potential Negative Impact.   The ease of deployment of our pose-free, zero-shot planar reconstruction model raises potential privacy concerns. Its ability to reconstruct 3D indoor scenes from sparse image pairs could be misused to capture private environments without consent, such as personal residences. While our model performs robustly across various datasets, rare failure cases may occur in challenging scenarios. In real-world deployments, integrating our model into a more comprehensive system is necessary to filter out occasional noisy predictions.